CORA Cork Open Research Archive
Cartlann Taighde Oscailte Chorcaí

Title	Compositional tuning of the aurivillius phase material Bi5Ti3–2xFe1+xNbxO15 (0 ⩽ x ⩽ 0.4) grown by chemical solution ddeposition and its influence on the structural, magnetic, and optical properties of the material
Authors	Halpin, Jennifer;Schmidt, Michael;Maity, Tuhin;Pemble, Martyn E.;Keeney, Lynette
Publication date	2020-05-25
Original Citation	Halpin, J. C., Schmidt, M., Maity, T., Pemble, M. E. and Keeney, L. (2021) 'Compositional Tuning of the Aurivillius Phase Material Bi5Ti3–2xFe1+xNbxO15 (0 ⩽ x ⩽ 0.4) Grown by Chemical Solution Deposition and its Influence on the Structural, Magnetic, and Optical Properties of the Material', IEEE Transactions on Ultrasonics, Ferroelectrics, and Frequency Control, 68(2), pp. 303-313. doi: 10.1109/TUFFC.2020.2997406
Type of publication	Article (peer-reviewed)
Link to publisher's version	https://ieeexplore.ieee.org/document/9099538 - 10.1109/TUFFC.2020.2997406
Rights	© 2020 IEEE. Personal use is permitted, but republication/ redistribution requires IEEE permission.
Download date	2026-11-05 13:40:17
Item downloaded from	https://hdl.handle.net/10468/11033

UCC
University College Cork, Ireland
Coláiste na hOllscoile Corcaigh

Compositional tuning of the Aurivillius phase material $Bi_5Ti_{3-2x}Fe_{1+x}Nb_xO_{15}$ ($0 \leq x \leq 0.4$) grown by chemical solution deposition and its influence on the structural, magnetic and optical properties of the material

Jennifer C. Halpin, Michael Schmidt, Tuhin Maity, Martyn E. Pemble and *Lynette Keeney

***Abstract*— A series of Aurivillius phase materials, $Bi_5Ti_{3-2x}Fe_{1+x}Nb_xO_{15}$ (x = 0, 0.1, 0.2, 0.3 and 0.4), was fabricated by chemical solution deposition. The effects of aliovalent substitution for the successful inclusion of Fe^{3+} and Nb^{5+} by replacing Ti^{4+} was explored as a potential mechanism for increasing magnetic ion content within the material. The structural, optical, piezoelectric and magnetic properties of the materials were investigated. It was found that a limit of $x = 0.1$ was achieved before the appearance of secondary phases as determined by X-ray diffraction. Absorption in the visible region increased with increasing values of x corresponding to the transition from the valence band to the conduction band of the Fe-e_g energy level. Piezoresponse force microscopy measurements demonstrated that the lateral piezoelectric response increased with increasing values of x. Magnetic measurements of $Bi_5Ti_{2.8}Fe_{1.1}Nb_{0.1}O_{15}$ exhibited a weak ferromagnetic response at 2K, 150 and 300K of 2.2, 1.6, 1.5 emu/cm^3 with Hc ~ 40, 36, 34 Oe respectively. The remanent magnetisation, M_R, of this sample was found to be higher than the range of reported values for the $Bi_5Ti_3Fe_1O_{15}$ parent phase. Elemental analysis of this sample by energy dispersive X-ray analysis did not provide any evidence for the presence of iron-rich secondary phases. However, it is noted that a series of measurements at varying sample volumes and instrument resolutions is still required to in order to put a defined confidence level on the $Bi_5Ti_{2.8}Fe_{1.1}Nb_{0.1}O_{15}$ material being a single-phase multiferroic.**

***Index Terms*—Aurivillius, ferroelectric, multiferroic, piezoelectric, thin films.**

Manuscript received February 28, 2020
This research was conducted with the financial support of the Royal Society and Science Foundation Ireland (SFI) University Research Fellowship UF 140263' and SFI project number 15/IA/3015: 'Design, Deposition and Exploitation of Novel Micro and Nano-scale Materials, 'DEPO-Man'.

J. Halpin is with Tyndall National Institute, University College Cork, Lee Maltings, Dyke Parade, Cork, Ireland and School of Chemistry, University College Cork, Cork, Ireland

M. Schmidt is with Tyndall National Institute, University College Cork, Lee Maltings, Dyke Parade, Cork, Ireland

T. Maity is with Dept. of Materials Science and Metallurgy, University of Cambridge, 27 Charles Babbage Road, Cambridge, CB3 0FS, U.K. and School of Physics, Indian Institute of Science Education and Research Thiruvananthapuram, Kerala 695551, India.

M. Pemble is with Tyndall National Institute, University College Cork, Lee Maltings, Dyke Parade, Cork, Ireland and School of Chemistry, University College Cork, Cork, Ireland

L. Keeney is with Tyndall National Institute, University College Cork, Lee Maltings, Dyke Parade, Cork, Ireland. *Corresponding author (e-mail: lynette.keeney@tyndall.ie).

I. Introduction

Multiferroic materials, possessing simultaneous ferroelectric (FE) and ferromagnetic (FM) order states, have been identified as leading contenders for enabling beyond CMOS data storage, whereby coupling between the FE and FM states permits energy-efficient switching of memory states and enhanced logic densities [1]. The unique advantage of these materials lies in the potential ability to simultaneously exploit both FE and FM memory states so as to facilitate the fabrication of multi-state storage devices [2]. In addition, the potential uses of multiferroics have broadened in recent times to include energy harvesting, photocatalytic and biomedical applications [3]. Development of true room-temperature multiferroic materials is difficult due to the competing electrical requirements for ferroelectricity and ferromagnetism [4]. The conventional route to ferroelectricity is to have cations with an empty *d* orbital, which enables hybridization between orbitals that stabilize the non-centrosymmetric polar structure; while ferromagnetism requires transition metals with partially filled *d* orbitals for exchange interactions to occur between unpaired electrons in nearby atoms [3]. This contraindication between the origins of ferromagnetism and ferroelectricity means that single-phase room temperature multiferroics are exceedingly rare and thus their material properties are currently limited. Attempts to overcome these contradictory requirements have included the creation of composite materials of a FE material and a FM material [5, 6]. An alternative approach is the design of single-phase materials that accommodate two different types of cations, possessing both empty and partially filled orbitals to drive both ferroelectricity and ferromagnetism, respectively. In this regard the Aurivillius phase family of materials provides a versatile scaffold in which both of these types of atoms can be accommodated. This family of materials is a homologous series of bismuth based, naturally layered oxides. They have the general formula $Bi_2O_2(A_{m-1}B_mO_{3m+1})$ and consist of $m$$ABO_3$ perovskite blocks separated by $[Bi_2O_2]^{2+}$ interlayers, with the primary growth axis along the c-axis direction. The chemical composition of the perovskite blocks can vary widely within certain size and valence constraints,

with the A-site occupied by a large 12-coordinate cation and the B-site occupied by a smaller 6-coordinate octahedral cation. This family of materials was first described by Aurivillius in 1949 [7] and since then have been utilized as high-temperature lead-free FEs due to their generally high Curie temperature (T_C > 500°C [8]) and more recently have been increasingly investigated as potential frameworks for magnetoelectric multiferroic materials.

Previous work from our group has demonstrated rare room temperature multiferroic behavior in the m = 5 Aurivillius system, $Bi_6Ti_xFe_yMn_zO_{18}$ (B6TFMO; x = 2.80 to 3.04; Y = 1.32 to 1.52; Z = 0.54 to 0.64) [9]. Thus far this is the only multiferroic material demonstrating intrinsic FE/FM properties to a defined confidence level (≥99.5%) in thin film form [10]. Our work has also demonstrated the reversible magnetoelectric switching necessary for practical magnetoelectric device applications [11]. In addition we have made significant advances in terms of understanding the fundamental mechanisms governing ferromagnetism in this material and why it is that manganese-containing samples in particular demonstrate multiferroic behavior [12]. Driven by strain- and electrostatic-energy factors, there is a marked preference for manganese cations to position themselves towards the center-most layer of the structure. This increases the probability of nearest neighbor magnetic interactions in the central layer by up to 90%. This tendency is pivotal in explaining pathways to long-range magnetic order and the distinct room temperature multiferroic properties of this tantalizing material system.

$Bi_4Ti_3O_{12}$ is a well-studied member of the Aurivillius family. It has three perovskite units (m=3) between the $[Bi_2O_2]^{2+}$ interlayers. The insertion of a $BiFeO_3$ unit, to produce the $Bi_5Ti_3Fe_1O_{15}$ composition (m=4), has been proposed as a route towards the creation of a multiferroic material [13]. Bismuth ferrite ($BiFeO_3$) is a well-known magnetoelectric multiferroic material [14]. The superexchange mechanism of magnetic coupling, common in insulating magnetic oxides, is a short-range mechanism involving virtual transfer of spin-polarized electrons [15]. Long range magnetic order, yielding a bulk magnetic signal throughout a sample, requires a sufficient concentration of magnetic ions to be located close to each other in the material. Increasing the concentration of magnetic ions in a material increases the probability of magnetic ions being near neighbors (NN) or next near neighbors (NNN) to each other. The theoretical occupancy of magnetic ions in the structure necessary for NN and NNN interaction has been calculated to be 31% and 14% respectively for a simple cubic lattice [16]. NN interactions produce a stronger magnetic response compared with NNN interactions and computational studies of the $Bi_5Ti_3FeO_{15}$ composition indicate that NN coupling constants of J_{NN} ~ 40–50 meV compared with NNN coupling constants of J_{NNN} ~ 1–2 meV [17]. Previous work has reported a weakly FM response in these $Bi_5Ti_3FeO_{15}$ materials [18, 19]. As well as potentially increasing the strength of the magnetic signal, computational studies have indicated that increasing the concentration of iron atoms should increases the temperature at which the material would exhibit magnetic behavior [20]. For these reasons it is desirable to increase the concentration of iron in $Bi_5Ti_3Fe_1O_{15}$. However, due to differences in valence and atomic radii of Ti^{4+} and Fe^{3+}, the ability to simply replace one with the other is limited and can lead to the formation of defects such as oxygen vacancies or stacking faults caused by intergrowths of alternating *m* values as the material reorders to accommodate the change in valence. This may also lead to the formation of associated secondary phase impurities. An essential requirement for the development of a multiferroic material is that the material is phase pure. Even trace (~0.01 vol. %) [10, 21] amounts of impurities present in the sample can be responsible for an observed magnetic response in the bulk material. Such trace levels of magnetic secondary phases are not generally detectable with analysis methods such as X-ray diffraction (XRD) because the noise level in any XRD scan places a limit on the detectability (typically 1-3 vol %). A careful investigation of possible impurity phases using detailed microstructural analysis (e.g. transmission electron microscopy (TEM), energy dispersive X-ray analysis (EDX), electron back-scattering detection etc.) together with statistical analysis is required in order to conclude with confidence that impurities are not affecting the measurements observed [10]. Without such rigorous analysis of sample purity, one cannot be confident that a material is truly a single-phase multiferroic.

Considering ionic valences and ionic radii, the co-substitution of Fe^{3+} and Nb^{5+} for Ti^{4+} has previously been proposed as a method to increase the incorporation of iron into the layered Aurivillius phases [17]. Co-substitution or aliovalent substitution of Fe^{3+} and Nb^{5+} at the Ti^{4+} site has been used in previous work on $Bi_5Ti_3FeO_{15}$ [22] and $Bi_4Ti_3O_{12}$ [23] materials fabricated using a solid state reaction method. Lavado *et al.* [23] reached a limit of x=0.5 ($Bi_4Ti_{3-2x}Nb_xFe_xO_{12}$) before secondary impurity phases were detected using XRD, having sub-threshold magnetic percolation (17%) to allow for long-range magnetic order with strong magnetic coupling. Chen *et al.* [22] did not see the expected increase in magnetic response even at 35% Fe occupation of the *B*-sites in the Aurivillius structure, which is above the theoretical percolation threshold for NN interactions. These ceramic materials were fabricated using solid state reaction methods.

Chemical solution deposition was used by Liu *et al.* to prepare a series of nanoparticulate materials of $Bi_5Ti_{3-x}Fe_{1+x}O_{15}$ [24] with Fe^{3+} substitution. No impurity peaks were detected by XRD in the compositions up to x = 0.6. The increased iron content was found to improve the visible light photodegradation of Rhodamine B dye solutions but the potential magnetic properties were not studied.

With these previous studies in mind, the objective of this present study is to attempt to systematically increase the concentration of Fe^{3+} ions in thin films of Aurivillius compound $Bi_5Ti_3FeO_{15}$ using aliovalent substitution of Fe^{3+} and Nb^{5+} ions at the Ti^{4+} ion sites, to create a series of thin film materials that have a generic formula of $Bi_5Ti_{3-x}Fe_{1+x}Nb_xO_{15}$. This has enabled a study of the structural properties of the resulting thin film materials to examine the influence of the materials composition and structure on the

observed magnetic percolation. To the best of our knowledge this study represents the first of its kind by clearly demonstrating weak FM behavior in an aliovalent substituted $Bi_5Ti_{2.8}Fe_{1.1}Nb_{0.1}O_{15}$ sample prepared via chemical solution deposition.

II. Experimental

Chemical solution deposition was the method used to fabricate the sample series; $Bi_5Ti_{3-2x}Fe_{1+x}Nb_xO_{15}$ (x = 0, 0.1, 0.2, 0.3 and 0.4). Details of this method are outlined in a previous publication [25] with the additional step of including niobium (Fig. 1). The precursors were weighed out in the proportions desired for the stoichiometry targeted. The bismuth precursor was present at 17.5% excess. This is a common precaution when using bismuth due to its volatility at the relatively high annealing temperatures used. Previous work on *m*=4 Aurivillius phases demonstrates that use of such an excess of bismuth mitigates the effects of bismuth migration and prevents the formation of secondary phase impurities such as pyrochlore $Bi_2Ti_2O_7$ [26]. The precursors $Bi(NO_3)_3.5H_2O$ (reagent grade, 98%, Sigma-Aldrich) and $Ti(OC_4H_9)_4$ (reagent grade, 97%, Sigma-Aldrich) were dissolved in lactic acid (ACS reagent, ≥85%, Sigma-Aldrich) at room temperature with constant stirring for a week to form Solution A. $Fe(NO_3)_3.9H_2O$ (ACS reagent, ≥98%, Sigma-Aldrich) and ($Nb(OC_2H_5)_5$) (99.9+%, Strem Chemicals, Inc.) were dissolved in acetylacetone (≥99.5% (Gas Chromatography grade), Sigma-Aldrich) to form Solution B. As the niobium precursor was moisture sensitive, these steps were performed in a nitrogen filled glove-bag. Solution B was slowly added to Solution A and was mixed thoroughly under nitrogen. The solution was then spin coated at 2000 rpm for 30 seconds onto c-plane sapphire substrates. Sapphire substrates were chosen for their cost-effectiveness and because they are chemically stable at the processing temperatures used to crystallize the Aurivillius phases. Although Si(100) and α-quartz are also cost-effective, previous studies [25] demonstrate that a reaction between the bismuth-containing Aurivillius phases and silicon tends to occur at the interface between film and substrate to form an amorphous Bi_2O_3-SiO_2 phase (e.g. $Bi_4Si_3O_{12}$) on cooling. The samples were baked at 300°C for 10 minutes on a hot plate in air to remove the residual organic solvents. The as-deposited materials were amorphous, and crystallization was induced by annealing at 850°C in a conventional furnace for 1 hour. The average film thickness was calculated to be 47 nm after measurements of 21 points across a section of the sample imaged by TEM, with the thickest region being 84 nm and the thinnest being 28 nm. A flow chart of the experimental procedure is shown in Fig. 1.

Details of analysis methods and instruments used during this study are as follows: XRD was performed with a Phillips Xpert PW3719 MPD diffractometer, Cu Kα radiation, 40 kV 35 mA, scan range 6° to 37.5°. Scanning electron microscopy (SEM) was performed using a Zeiss Supra 40 instrument.

Atomic Force Microscopy (AFM) and Piezoresponse Force Microscopy (PFM) were performed using an MFP-3D™ Asylum Research instrument. AFM was conducted in AC mode using Olympus AC240TS probes (Al reflex coated, 15 nm tip radius, 70 kHz resonant frequency). PFM was conducted in both single frequency and lateral Dual AC Resonance Tracking (DART-PFM) mode [27]. The DART-PFM mode was used to boost the vertical piezo signal. In this mode, the PFM signal is measured at the tip-sample contact resonance frequency, where the drive frequencies are adjusted as the probe scans over the changing sample topography in order to reduce topographical cross-talk. The probes used were Olympus AC240TM electrilevers (Ti/Pt coated silicon probes, Al reflex coated, 15 nm tip radius, 70 kHz resonant frequency)).

Transmission measurements in the ultra violet - visible (UV-vis) range were performed on a Perkin Elmer λ950 spectroscope with an integrated sphere attachment and direct reflectance was measured on the same instrument using a Universal Reflectance Accessory. Diffuse reflectance was measured using a Shimadzu UV-2401 PV UV-vis recording spectroscope. The percentage absorption was calculated using the relationship $A\% = 100 - T\% - (R\%_{direct} + R\%_{diffuse})$.

For high resolution TEM (HR-TEM) cross-sections of the films were prepared for micro-structural analysis using a FEI DualBeam Helios NanoLab 600i Focussed Ion Beam (final thinning at 93 pA 30 kV, final polish 5 kV 47 pA). Micro-structural analysis was performed using HR-TEM (Jeol 2100 transmission electron microscope; 200 kV; double tilt holder).

EDX spectra were obtained using a FEI Helios Nanolab High-Resolution Scanning Electron Microscope with attached Oxford X-Max 80 detector and Aztec analysis software.

The magnetic measurements were carried out in Quantum

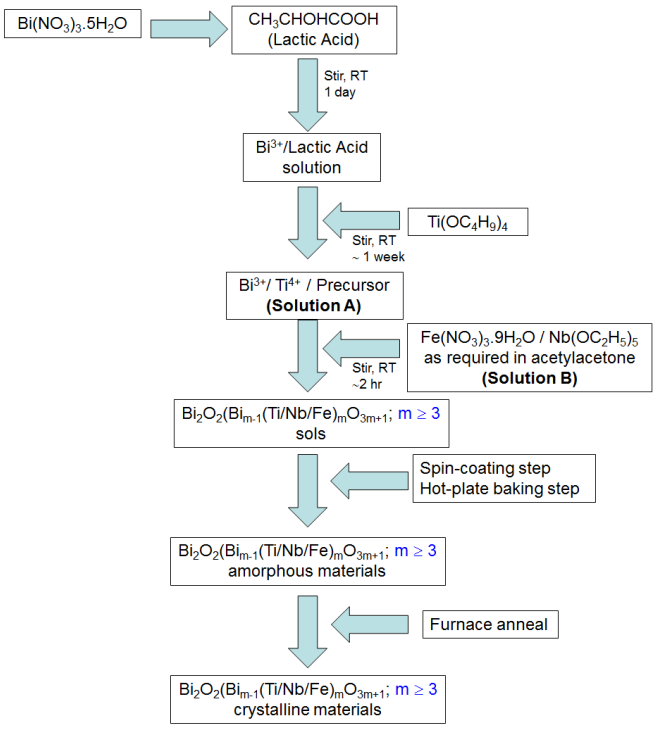


Fig.1. Flow chart depicting the experimental steps involved in preparing the $Bi_5Ti_{3-x}Fe_{1+x}Nb_xO_{15}$ (m=4) Aurivillius sample series by chemical solution deposition.

Design's MPMS 3 magnetometer (±70 kOe field range, 1.8 – 400K temperature range). Before each measurement the samples were demagnetized using an appropriate demagnetization protocol [28]. The hysteresis loops (MH curves) were measured at ±70 kOe field range at different temperatures. The temperature dependent magnetization (MT) was measured at a 10K/min cooling rate.

III. Results and Discussion

A sample series $Bi_5Ti_{3-2x}Fe_{1+x}Nb_xO_{15}$ with x = 0, 0.1, 0.2, 0.3 and 0.4 (hereafter referred to as Bi5Nb0, Bi5Nb0.1, etc.) was fabricated using chemical solution deposition on c-plane sapphire substrates. The as-deposited samples were amorphous and light brown in color. After annealing at 850°C for 1 hour the samples underwent a structural change to form the crystal structure accompanied by a color change to pale yellow. XRD of the sample series confirmed the formation of the *m*=4 Aurivillius material. There was a preferred orientation for the growth axis perpendicular to the substrate, in the *c*-axis direction, with a majority of the peaks corresponding to (00l) reflections (Fig. 2). As will be shown in AFM, SEM and TEM images, a number of the Aurivillius plates lie at an angle to the substrate which accounts for the small (020) reflection observed (Fig. 3 (a)). This peak is most intense for the x =0.2 sample. We note that there is a general decrease in the intensity of the peaks corresponding to the m = 4 Aurivillius phase as *x* increases. The Lotgering factor [29] provides a measure of the texture of the samples. The Lotgering factor f is given by,

$$f = \frac{P - P_0}{1 - P_0} \qquad (1)$$

where,

$$P = \frac{\sum I(00l)}{\sum I(hkl)} \quad \text{and} \quad P_0 = \frac{\sum I(00l)_0}{\sum I(hkl)_0} \qquad (2)$$

Here, ∑I(00l) is the sum of the intensities of all (00l) reflections, ∑I(hkl) is the sum of the intensities from all the peak reflections of the material and $\sum I(00l)_0$ and $\sum I(hkl)_0$ are the corresponding values from a randomly oriented sample. The intensities of a randomly oriented sample were obtained from the XRD values generated by using VESTA software [30] from the data provided by Lui *et al.* in their paper on $Bi_5Ti_3FeO_{15}$ materials [24]. There was a small decrease in the Lotgering factor between samples Bi5Nb0 (f = 0.996) and Bi5Nb0.1 (f = 0.991), indicating a small structural change occurred upon substitution of Fe and Nb.

The Bi5Nbx series was indexed from a simulated XRD plot generated by using VESTA software [30] from the data provided by Lui *et al.* [24]. This corresponded to the orthorhombic space group $A2_1am$. As the concentration of Fe^{3+} and Nb^{5+} increases, the intensity of the peaks tends to decrease and peaks broaden and shift position. The peak shift is accompanied by the appearance of the (222) and possibly the (444) reflection of the pyrochlore bismuth titanium oxide ($Bi_2Ti_2O_7$) phase (JCPDF 32-0118) at 14.6° and 29.6° in the Bi5Nb0.2, Bi5Nb0.3 and Bi5Nb0.4 samples. The formation of this secondary phase indicates that stoichiometric $Bi_5Ti_{2.6}Fe_{1.2}Nb_{0.2}O_{15}$, $Bi_5Ti_{2.4}Fe_{1.3}Nb_{0.3}O_{15}$, and $Bi_5Ti_{2.2}Fe_{1.4}Nb_{0.4}O_{15}$ compositions have not been formed. Small peaks (at 2theta positions of 10.6° and 16.0°) indicate the formation of the m=3 Aurivillius phase $Bi_4Ti_3O_{12}$ (JCPDF 35-0795) which can be seen in samples with x > 0.1 Another strong reflection (008) expected for this (m=3) phase at 21.6° would overlap with the (00<u>10</u>) reflection of the m=4 phase. Note that no peaks corresponding to the haematite phase, Fe_2O_3 (JCPDF 89-0599), were observed ((220) reflection occurs at ~ 33.2°) within the detection limit of the instrument (typically 1-3 vol %). The magnetite spinel phase, Fe_3O_4 (JCPDF 89-0951), has a (311) reflection at ~ 35.4° which overlaps with the *m*=4 (00<u>16</u>) reflection. A peak at 29.6°, seen in samples $Bi_5Nb_{0.2}$ and $Bi_5Nb_{0.3}$, aligns with the (220) reflection of magnetite. This occurs in the same range as the (444) reflection of pyrochlore $Bi_2Ti_2O_7$, therefore it is not

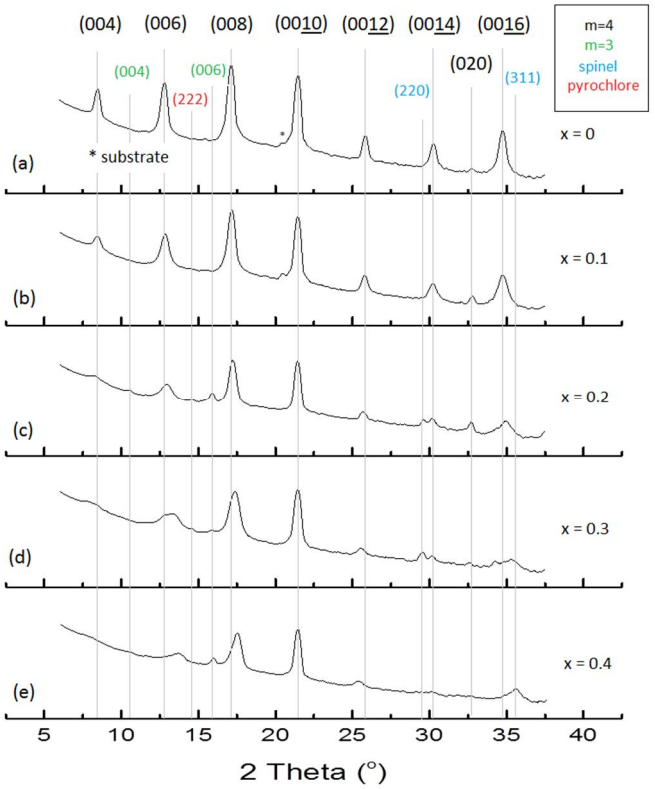


Fig. 2. XRD graphs of the Bi5Nb series (a) Bi5Nb0, (b) Bi5Nb0.1, (c) Bi5Nb0.2, (d) Bi5Nb0.3, (e) Bi5Nb0.4. $Bi_5Ti_3Fe_1O_{15}$ m = 4 space group $A2_1am$ (black), $Bi_4Ti_3O_{12}$ m=3 space group $B2cb$ (green), pyrochlore $Bi_2Ti_2O_7$ space group $Fd3m$ (red) and spinel Fe_3O_4 space group $Fd3m$ (blue).

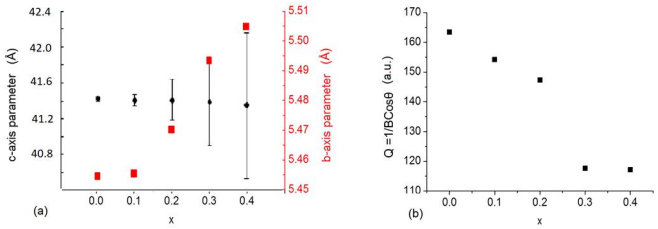


Fig. 3. The *b* and *c*–axis parameters (a) and the relative crystalline quality factor (b) calculated form XRD measurements.

possible to definitively assign this peak. Considering the observed presence of secondary phases in samples of *x* greater than 0.1, subsequent characterisation of FE and FM properties focused on the *x*=0.1, $Bi_5Nb_{0.1}$ sample.

The *b* and *c*-axis lattice parameters were calculated from the XRD measurements using the following relationship (3) between the lattice parameters of the orthorhombic system and the interplanar distances from the Bragg condition.

$$\frac{1}{d^2} = \frac{h^2}{a^2} + \frac{k^2}{b^2} + \frac{l^2}{c^2} \qquad (3)$$

As there was no (*h*00) reflection over this scan range it was not possible to calculate the *a*-axis lattice parameter. The *b*-axis lattice parameter, which increases with Fe^{3+} and Nb^{5+} addition, was calculated from a single (020) reflection. It was found that the error associated with the calculated *c*-axis lattice parameter becomes significant above values of *x*=0.1 (Fig. 3 (a)). This can be attributed to the decrease in sample purity and the occurrence of secondary phases having d-spacings similar to the *m*=4 Aurivillius phase. There is a general decrease in the intensity and sharpness of the peaks corresponding to the *m*=4 Aurivillius phase as *x* increases. If we take a value for the *a*-axis parameter of 5.4698 Å from the detailed work of Hervoches *et al.* [31] we calculate a unit cell volume of 1237.83 and 1236.36 $Å^3$ for Bi5Nb0 and Bi5Nb0.1, respectively. This is comparable to the values obtained by Chen *et al.* [22] for the ceramic materials of similar composition. The Goldschmidt tolerance factor (*t*) was calculated for the series and decreased from 0.8539 to 0.8526 for *x* = 0 to *x* = 0.4. *t* is a measure of the tilt of the perovskite unit [32]. Insertion of larger atoms at the *B*-site of the perovskite blocks changes bond lengths in the structure causing increased rotation of the perovskite octahedra [33].

As the Aurivillius materials are orthorhombic and not cubic, the Scherrer equation could not be used to estimate particle size but instead was used in modified form to provide a measure of the crystalline quality of the materials. The relative crystalline factor (Q) was derived from a modified form of the Scherrer equation (4) [34].

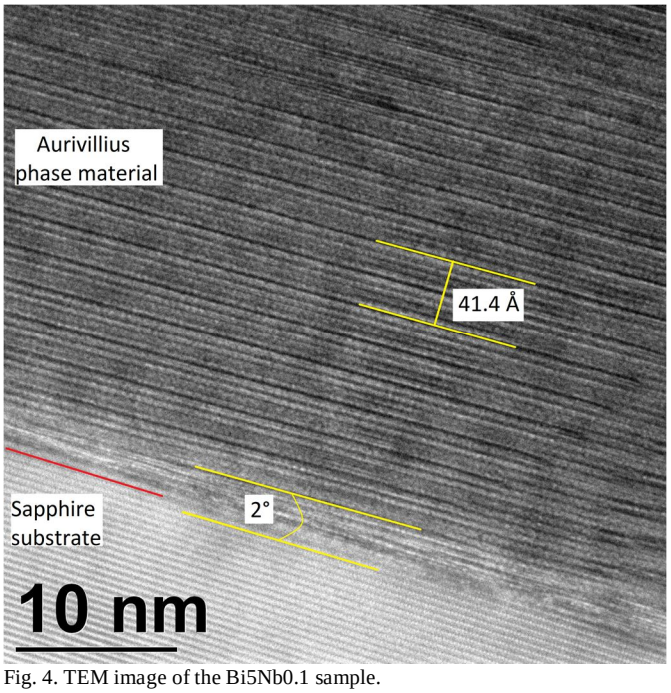


Fig. 4. TEM image of the Bi5Nb0.1 sample.

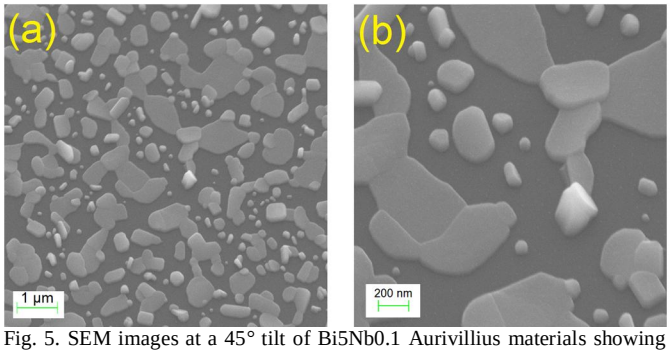


Fig. 5. SEM images at a 45° tilt of Bi5Nb0.1 Aurivillius materials showing the plate like grains that predominantly lie parallel to the substrate.

$$Q = \frac{1}{\beta Cos\theta} \qquad (4)$$

Where β is the FWHM (full width at half maximum) (in radians) and θ is the angle of diffraction. The averaged FWHM of the (008), (00$\underline{1}$0) and (00$\underline{1}$2) peaks were used in the calculation (Fig. 3 (b)). The value of Q decreased with increasing Fe and Nb concentration. This was as expected due to the formation of secondary phases at higher Fe and Nb concentrations. An abrupt decrease in the value of Q for the Bi5Nb0.3 and Bi5Nb0.4 samples corresponds to the appearance of significant secondary phases in the XRD patterns of these materials. This further supports that a solution limit of x = 0.1 was reached for this series.

A typical TEM image of the $Bi_5Nb_{0.1}$ sample is shown in Fig. 4. From the TEM measurements, unit cell thickness was measured to be 41.4 Å compared to a c-axis parameter value of 41.40 Å calculated from XRD measurements. An error of (at least) 10% should be applied to measurements taken from the TEM images. The thickness of the plates measured ranged from 28 to 84 nm. This corresponds to a range of 8 to 20 unit cells in the plate like grains. Both the Aurivillius phase and the sapphire substrate are crystalline, but they are not lattice matched. The pseudo-cubic lattice parameter for $Bi_5Nb_{0.1}$ (calculated by the method of [35]) is 3.88 Å, which is considerably different to the lattice constant *a* = 4.78 Å for sapphire (+23.20% lattice mis-match). The sapphire substrate therefore acts simply as a mechanical support for the

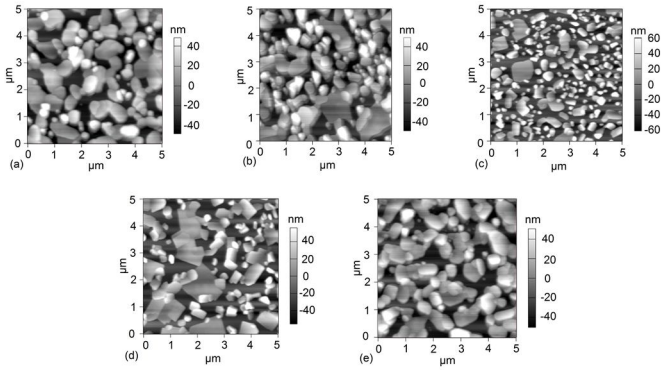


Fig. 6. AFM topography images (a) Bi5Nb0, (b) Bi5Nb0.1, (c) Bi5Nb0.2, (d) Bi5Nb0.3 and (e) Bi5Nb0.4.

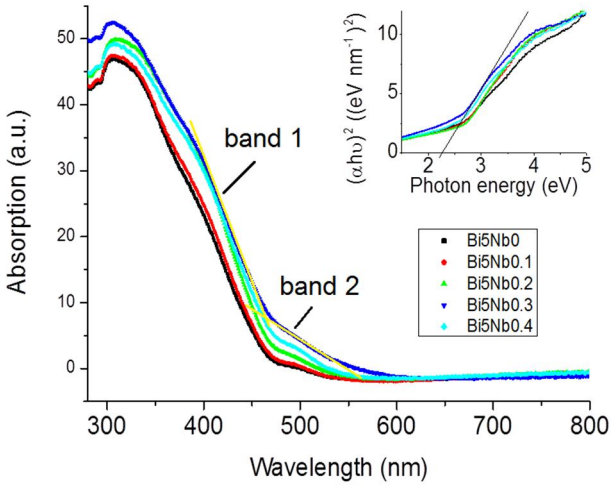


Fig.7. Absorption spectra for the Bi5Nb series. The insert displays the Tauc plot.

Aurivillius materials and there is no epitaxial relationship affecting crystal growth. SEM (Fig. 5) and AFM (Fig. 6) images demonstrate that film coverage was not continuous over the sample surface and several grains lie partially on top of each other. This overlapping tendency of the grains means that several plates are tilted at the region where they meet and lie at an angle with respect to the substrate surface. For example, the image presented in Fig. 4 demonstrates that for the region of the sample imaged, the c-axis was inclined at an angle of approximately 2° with respect to the substrate.

The topography of the material was examined using SEM and AFM. Analysis of the amorphous materials before annealing showed there was complete coverage over the substrate. During crystallization the materials contracted exposing the substrate underneath. SEM images show the characteristic plate like grains common for Aurivillius materials (Fig. 5). A majority of plates lie parallel to the sapphire substrate but some are positioned at an angle where plates overlap.

From AFM measurements of the sample series (Fig. 6) the average percentage coverage was found to be between 54-72% for the Bi_5Nb_x series and the RMS roughness between 26-30 nm. There was no significant trend observed through the sample series as the average values obtained for each sample fell within the standard deviation error of the other samples in that series.

Since there has been a growing interest in the use of $Bi_5Ti_3Fe_1O_{15}$ materials as photocatalytic materials, the optical properties of the materials synthesized here were also investigated. Two major challenges to the development of photocatalytic materials are: that the materials absorb in the visible light region of the solar spectrum and that charge separation occurs within the materials. The Aurivillius materials such as $Bi_5Ti_3FeO_{15}$ are attractive candidates for use as photocatalysts as they generally absorb in the visible region and are naturally layered materials [36, 37]. Layered materials have been noted as having good charge separation capabilities which prevents the separated charges recombining before the catalytic reaction such as water splitting can occur [38, 39].

In Fig. 7 the absorption spectra for the sample series is shown. Similar to previous work [24, 40] two clear absorption

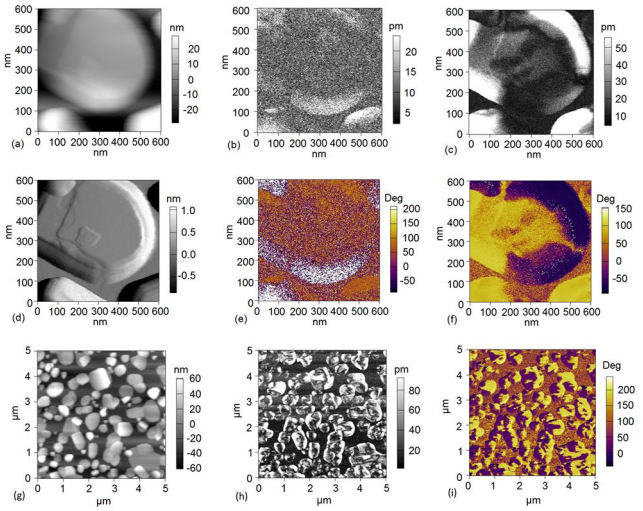


Fig.8. Single frequency PFM measurements of $Bi_5Ti_{2.8}Fe_{1.1}Nb_{0.1}O_{15}$, (a) height, (b) vertical amplitude, (c) lateral amplitude, (d) vertical deflection, (e) vertical phase and (f) lateral phase. Representative lateral DART PFM images (g) height, (h) amplitude and (i) phase of Bi5Nb0.1 sample.

bands can be seen. Band 1 (400-460 nm) corresponds to the transition from the valence band (VB) to the Ti3*d* conduction band (CB). The VB of these $Bi_5Ti_3Fe_1O_{15}$ samples was determined to be made up of O2p + Fe-t_{2g} + Bi6s energy levels [41]. Band 2 corresponds to the transition from the VB to CB of Fe-e_g. This is a smaller energy difference and so occurs at higher wavelengths 470-530 nm.

Values of the band gap energy were obtained from extrapolation of the inflection point of an associated Tauc plot (5) [42],

$$(\alpha h\upsilon) = B(h\upsilon - E_G)^n \quad (5)$$

where E_G is the band gap energy (eV), hν is photon energy (eV) and B is a scaling constant and n = 1 or 1/2 for direct and indirect transition respectively. Band gap values of 2.17 eV, 2.3 eV, 2.38 eV, 2.19 eV, and 2.23 eV were obtained for Bi5Nb0 to Bi5Nb0.4, respectively. These band gaps were found from the extrapolation of the inflection point relating to band 1. No significant change in band gap was observed upon Fe and Nb substitution. In previous reports, E_G values of 2.03 eV [43], 2.38 eV [37], 2.59 eV [24] and 3.31 eV [44] were obtained for $Bi_5Ti_3FeO_{15}$ materials. It is important to note that

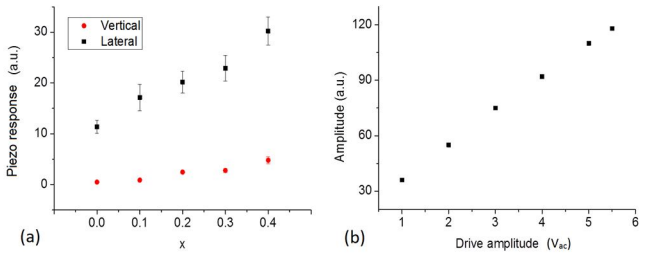


Fig. 9. (a) Relative piezoresponse in the lateral and vertical direction for the Bi5Nbx sample series. The error bars represent the standard deviation between measurements at five different areas on the sample. (b) The lateral piezoresponse as a function of increasing drive amplitude of sample Bi5Nb0.1. Note that the piezoresponse has not been normalized to pm/V, it has been displayed in picometers (pm) to allow for the change in the piezoresponse as a function of voltage to be demonstrated.

the morphology of the material can impact on the absorption of light and variations in sample coverage and roughness through the series may contribute to variations observed in the calculated band gap values. With increased substitution, the absorption was found to increase in the region of band 2. Absorption of wavelengths at 500 nm increased by ~ 5% for the Bi5Nb0.3 sample.

The $Bi_5Ti_3Fe_1O_{15}$ Aurivillius materials are well known FEs. The primary polarization axis is along the a/b direction parallel to the $[Bi_2O_2]^{2+}$ interlayer [45]. Single frequency measurements (measurement frequency 15 kHz) of simultaneous lateral and vertical response (Fig. 8 (a-f)) clearly demonstrate the expected anisotropy of the polarization. Simultaneous single frequency measurements (measurement frequency 15 kHz) show a much larger response in the lateral direction relative to the vertical direction (Fig. 9(a)). The linearity of lateral piezoresponse (pm) with drive amplitude (V_{ac}) was verified to support piezoelectric behavior (Fig. 9(b)). The presence of a small vertical response can be attributed to the fact that not all the grains are lying parallel to the substrate in the c-axis direction (see Fig. 2). Furthermore, grain overlaps can be observed (Figs 5 and 6) leading to an out-of-plane tilt of the Aurivillius plate-like grain whereby the vertical PFM tip has access to the in-plane polarization component [46]. As seen in the TEM analysis (Fig 4), some of the plates do not lie parallel to the substrate.

An increasing piezoresponse in both the lateral and vertical directions was observed with increased substitution. This increase may be due to the increased distortion of the perovskite units shown by the increase in *b*-axis lattice parameter which arises as the larger atoms (Fe or Nb) are substituted for Ti [33]. Lattice distortion was also reflected in slight changes in the *a* and *b* lattice parameters of a W/Cr co-substituted $Bi_4Ti_3O_{12}$ Aurivillius system [47]. The distortion of the perovskite lattice due to octahedral rotation is well known to affect the polarization behavior of the Aurivillius materials [33]. An inverse relationship exists, where the Curie temperature (T_C) and the Goldschmidt tolerance factor were found to increase and as *t* decreases [32]. In previous work, insertion of ions leading to an increased distortion of the perovskite unit resulted in an increase in the polarization coefficients [48, 49]. A decrease in lattice distortion was found to decrease the polarization coefficients [50].

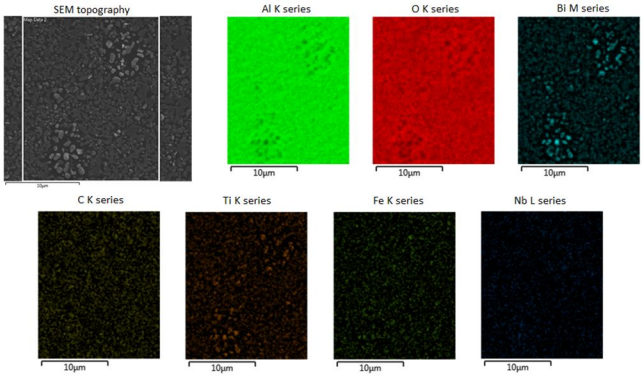


Fig. 11. Surface SEM topography and EDX surface analysis of the Bi5Nb0.1 sample.

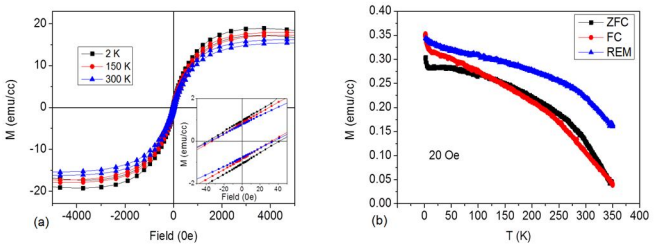


Fig. 10. (a) MH curves after subtraction of the diamagnetic contribution of the substrate magnetic measurements for Bi5Nb0.1. A small magnetic signal of approximately 2.2, 1.6 and 1.5 emu/cm^3 and a Hc ~ 40, 36, 34 Oe at 2, 150 and 300K was detected under zero applied magnetic field (inset (a)). (b) MT graph showing the zero field cooled (ZFC), field cooled (FC) and remnant (REM) curves.

Given the relatively low piezoresponse, topography cross-talk is likely also to have some contribution to the single frequency vertical PFM images obtained. Imaging of Bi5Nb0.1 with lateral DART-PFM (Fig. 8 (g-i)) mode reduces topography cross talk and amplifies the piezoresponse. The average response of the negatively polarized domains differs to that of the positive ones, indicating that these films are naturally self-polarized. Clear grain boundaries can be seen. All samples in the Bi5Nb series demonstrated piezoelectric behavior and there were no observable differences in the DART-PFM images of the different samples in the series.

The theoretical concentration of iron atoms over the four available B-sites in the structure is 25%, 27.5%, 30%, 32.5% and 35% for x = 0, 0.1, 0.2, 0.3, 0.4, respectively. For a random distribution of atoms throughout the four B-sites available, the probability of strong nearest neighbor (NN) coupling requires 31% occupation and 14% occupation is required when considering both weak next-nearest neighbor (NNN) coupling and NN coupling [16]. NNN results in a weak magnetic response compared to NN interactions. Therefore a stronger magnetic signal would be expected for Bi5Nb0.3 and Bi5Nb0.4. However, it is clear from XRD measurements that secondary phases occur at concentrations of $x \geq 0.2$ making them unsuitable for magnetic analysis. Therefore the Bi5Nb0.1 sample was chosen for magnetic measurements as secondary phases were not observed for this sample during bulk XRD measurements. Unsaturated magnetic hysteresis loops (MH curves) were obtained for this sample when measured at temperatures of 2, 150 and 300 K. The sample shows weak FM behavior at all three temperatures (Fig. 10(a)). The remanent magnetization (M_R) was measured as 2.2 emu/cm^3 or 0.28 emu/g at 2K, 1.6 emu/cm^3 or 0.2 emu/g at 150 K and 1.5 emu/ cm^3 or 0.19 emu/g at 300K. M_R can be influenced by extrinsic factors such as grain size and orientation; therefore, it can be difficult to compare results with different fabrication methods. This can help to explain the variation in reported values of M_R in the literature. Thin films of $Bi_6Ti_{2.8}Fe_{1.52}Mn_{0.68}O_{18}$ fabricated using a very similar experimental procedure exhibited a comparable magnetic response of M_R=0.18emu/cm^3 and saturation magnetization (M_S)= 6.05 emu/cm^3 at 300K [9]. Mao *et al.* observed a significant difference in samples of $Bi_5Ti_3FeO_{15}$ prepared by a multi-calcination procedure compared to the traditional solid-

state reaction method [51]. While Song *et al*. also observed differences between their six perovskite layered materials, fabricated by chemical solution deposition, and previous literature reports [52]. $Bi_5Ti_3Fe_1O_{15}$ prepared by conventional solid state reaction was found to have a weak FM response of M_R=0.122 memu/g [53] and 1.36 × 10^{-3} memu/g [19]. For previously reported $Bi_5Ti_3Fe_1O_{15}$ thin films fabricated by chemical solution deposition, M_S = 1.7 emu/cm^3 [54], 0.21 emu/cm^3 [43] and 0.21 emu/ cm^3 [44] were reported.

It must be noted that a purity assessment of the samples used for magnetic measurements seldom accompanies the reported magnetization values. Trace (~0.01 vol.%) [10, 21] amounts of undetected impurities present in the sample may be responsible for the variance in magnetization values reported.

The coercivity (H_C) was measured as being ~40 Oe at 2K, which slightly decreases with increase of temperature (Fig. 10 (a)). The magnetization was examined as a function of decreasing temperature (Fig. 10 (b)) with an applied field of 20 Oe. The difference between the field-cooled (FC) and zero field cooled (ZFC) curve below 100 K clearly indicates a FM response from a single magnetic phase. This is also confirmed by the remanence (REM) magnetization curve, which is positive and decreases with increase of temperature. This work confirms FM behavior at room temperature and above (up to 350K as experimented), indicating the potential use of the Bi5Nb0.1 material for room temperature multiferroic device applications. Based on a *B*-site iron occupation of 27.5% for this sample, the magnetic response observed can be attributed to weak NNN interactions, if the iron is randomly distributed over the available B-sites. However, experimental [12, 55] and computational [17] studies have indicated that the partitioning of Fe ions throughout the Aurivillius structure is not evenly distributed over all available perovskite layers and that preferential magnetic ion partitioning may increase magnetic percolation within particular perovskite layers. There are two non-equivalent *B*-sites present in the m = 4 structure. The outer perovskite layers are adjacent to the $(Bi_2O_2)^{2+}$ interlayer and experience a different environment compared to the two inner perovskite layers. There is an electrostatic preference for the more-highly-charged Ti^{4+} to occupy the outer sites close to the outer layer of oxygen ions in the $[Bi_2O_2]^{2+}$ [56]. There is also a strain energy which serves to drive cations larger than Ti^{4+} away from the layers closest to the $[Bi_2O_2]^{2+}$ layers [35, 57]. This would concentrate the iron atom to the inner perovskite blocks. Similar partitioning of Cr was observed in $Bi_5Ti_3CrO_{15}$ systems as demonstrated by neutron diffraction experiments [58]. Theoretical calculations [17] indicate that the strength of the NN couplings for magnetic cations located within inner sites (J_{NN} ~43 to 46 meV) is more than twice that for adjacent inner to outer site (J_{NN} ~12 to 20 meV) NN coupling interactions, therefore distribution of magnetic cations within these inner layers is crucial to the percolation and strength of magnetic interactions within the Aurivillius phases.

The super exchange interaction between Fe^{3+} - Fe^{3+} atoms would be predicted to give rise to antiferromagnetic behavior. However, the MH relationship for an antiferromagnetic behavior is linear [23]. It is possible that the FM response observed here is due to a Fe^{3+}-Fe^{2+} super exchange mechanism. Another possible cause for the weak ferromagnetism might be that it arises from spin canting, as described for $BiFeO_3$ [19, 56]. The H_C (Fig. 10(a)) and the magnetization (Fig. 10(b)) decrease with an increase in temperature (T) for Bi5Nb0.1 which is similar to the model system $BiFeO_3$ and other multiferroic ferromagnets [28, 59, 60]. Given the relatively weak FM signal observed for Bi5Nb0.1, changes in H_C and M_R as a function of temperature are relatively small.

The exact same Bi5Nb0.1 sample piece that was used for magnetic measurements was then analysed by surface SEM/EDX (Fig 11). Scans of the sample did not show any micron-sized observable Fe clusters which could indicate secondary impurity phases such as Fe_2O_3 or the magnetic spinel phase Fe_3O_4. Considering the observed magnetic signal at 300K was 0.19 emu/g, the presence of just 0.0095 vol. % of Fe_3O_4 in the sample could be responsible for this weak magnetic signal. Based on the EDX data we have, we can rule out inclusions greater than 3 μm contributing significantly to the magnetic signal measured. It would be necessary to perform the procedure developed by Schmidt *et al.* to put a defined confidence level on a material being a single phase material. This would require a series of measurements at varying sample volumes and instrument resolutions and full statistical analysis [10].

IV. Conclusion

In this work a series of Aurivillius phase materials were synthesized using chemical solution deposition which was found to be a facile, relatively simple way to control the material stoichiometry. The following samples were prepared; $Bi_5Ti_{3-x}Fe_{1+x}Nb_xO_{15}$ with x = 0, 0.1, 0.2, 0.3, 0.4. Using aliovalent substitution the concentration of Fe and Nb was increased in the material while the Ti concentration decreased. The effects of the variation in stoichiometry on the physical, optical and electrical properties were examined. The change in lattice parameters was attributed to the insertion of larger atoms at the *B*-site of the perovskite and the resulting increase in distortion of the perovskite unit. The majority of peaks corresponded to 00*l* reflections. However the formation of additional secondary phases indicates that substitution after x = 0.1 is not stoichiometric. This suggests a solution limit of x = 0.1 for this series. The increase in Fe and Nb substitution was found to increase the absorption of visible light in the region 470-530 nm. Using PFM it was established that as expected, the major polarization was along the a/b axis. The piezoresponse was found to increase with increased Fe and Nb substitution in both the lateral and vertical direction, indicating that the FE behaviour of the material was enhanced, and not adversely affected by the magnetic ion substitution. A small FM response was observed at room temperature for the Bi5Nb0.1 sample, which is desirable for multiferroic device applications. The magnitude of the M_R response was found to be higher than the range of reported values for the

$Bi_5Ti_3Fe_1O_{15}$ parent phase; however extrinsic factors such as sample fabrication methods make comparison difficult. While EDX analysis did not show any iron-rich impurity inclusions in this sample, the possibility of an inhomogeneous distribution of secondary impurity phases cannot be dismissed due to the limit of detection of the analysis methods used thus far.

V. References

[1] S. Manipatruni, D. E. Nikonov, C. C. Lin, T. A. Gosavi, H. Liu, B. Prasad, *et al.*, "Scalable energy-efficient magnetoelectric spin-orbit logic," *Nature*, vol. 565, pp. 35-42, Jan 2019.

[2] F. Yang, M. H. Tang, Z. Ye, Y. C. Zhou, X. J. Zheng, J. X. Tang, *et al.*, "Eight logic states of tunneling magnetoelectroresistance in multiferroic tunnel junctions," *Journal of Applied Physics*, vol. 102, p. 044504, 2007/08/15 2007.

[3] N. A. Spaldin and R. Ramesh, "Advances in magnetoelectric multiferroics," *Nat Mater*, vol. 18, pp. 203-212, Mar 2019.

[4] N. A. Hill, "Why Are There so Few Magnetic Ferroelectrics?," *The Journal of Physical Chemistry B*, vol. 104, pp. 6694-6709, 2000/07/01 2000.

[5] C.-W. Nan, M. I. Bichurin, S. Dong, D. Viehland, and G. Srinivasan, "Multiferroic magnetoelectric composites: Historical perspective, status, and future directions," *Journal of Applied Physics*, vol. 103, p. 031101, 2008/02/01 2008.

[6] H. Palneedi, V. Annapureddy, S. Priya, and J. Ryu, "Status and Perspectives of Multiferroic Magnetoelectric Composite Materials and Applications," *Actuators*, vol. 5, 2016.

[7] B. Aurivillius, "Mixed bismuth oxides with layer lattices. 2. Structure of Bi4Ti3O12," *Arkiv for Kemi*, vol. 1, pp. 499-512, 1950.

[8] N. A. Lomanova, M. I. Morozov, V. L. Ugolkov, and V. V. Gusarov, "Properties of aurivillius phases in the Bi4Ti3O12-BiFeO3 system," *Inorganic Materials*, vol. 42, pp. 189-195, 2006.

[9] L. Keeney, T. Maity, M. Schmidt, A. Amann, N. Deepak, N. Petkov, *et al.*, "Magnetic Field-Induced Ferroelectric Switching in Multiferroic Aurivillius Phase Thin Films at Room Temperature," *Journal of the American Ceramic Society*, vol. 96, pp. 2339-2357, 2013/08/01 2013.

[10] M. Schmidt, A. Amann, L. Keeney, M. E. Pemble, J. D. Holmes, N. Petkov, *et al.*, "Absence of Evidence ≠ Evidence of Absence: Statistical Analysis of Inclusions in Multiferroic Thin Films," *Scientific Reports*, vol. 4, p. 5712, 2014/07/16 2014.

[11] A. Faraz, T. Maity, M. Schmidt, N. Deepak, S. Roy, M. E. Pemble, *et al.*, "Direct visualization of magnetic-field-induced magnetoelectric switching in multiferroic aurivillius phase thin films," *Journal of the American Ceramic Society*, vol. 100, pp. 975-987, 2017.

[12] L. Keeney, C. Downing, M. Schmidt, M. E. Pemble, V. Nicolosi, and R. W. Whatmore, "Direct atomic scale determination of magnetic ion partition in a room temperature multiferroic material," *Sci Rep*, vol. 7, p. 1737, May 11 2017.

[13] F. Kubel and H. Schmid, "X-ray room temperature structure from single crystal data, powder diffraction measurements and optical studies of the aurivillius phase Bi5(Ti3Fe)O15," *Ferroelectrics*, vol. 129, pp. 101-112, 1992.

[14] C. Ederer and N. A. Spaldin, "Weak ferromagnetism and magnetoelectric coupling in bismuth ferrite," *Physical Review B*, vol. 71, p. 060401, 02/08/ 2005.

[15] L. W. Martin, Y. H. Chu, and R. Ramesh, "Advances in the growth and characterization of magnetic, ferroelectric, and multiferroic oxide thin films," *Materials Science and Engineering: R: Reports*, vol. 68, pp. 89-133, 2010.

[16] Ł. Kurzawski and K. Malarz, "Simple Cubic Random-Site Percolation Thresholds for Complex Neighbourhoods," *Reports on Mathematical Physics*, vol. 70, pp. 163-169, 10// 2012.

[17] A. Y. Birenbaum and C. Ederer, "Potentially multiferroic Aurivillius phaseBi5FeTi3O15: Cation site preference, electric polarization, and magnetic coupling from first principles," *Physical Review B*, vol. 90, 2014.

[18] A. Srinivas, S. V. Suryanarayana, G. S. Kumar, and M. M. Kumar, "Magnetoelectric measurements on and," *Journal of Physics: Condensed Matter*, vol. 11, pp. 3335-3340, 1999/01/01 1999.

[19] X. Y. Mao, W. Wang, and X. B. Chen, "Electrical and magnetic properties of Bi5FeTi3O15 compound prepared by inserting BiFeO3 into Bi4Ti3O12," *Solid State Communications*, vol. 147, pp. 186-189, 2008/08/01/ 2008.

[20] A. Yaël Birenbaum, A. Scaramucci, and C. Ederer. (2016, December 01, 2016). Magnetic order in 4-layered Aurivillius Phases. *arXiv e-prints*. Available: https://ui.adsabs.harvard.edu/abs/2016arXiv161207343Y

[21] A. Faraz, J. Ricote, R. Jimenez, T. Maity, M. Schmidt, N. Deepak, *et al.*, "Exploring ferroelectric and magnetic properties of Tb-substituted m=5 layered Aurivillius phase thin films," *Journal of Applied Physics*, vol. 123, Mar 2018.

[22] C. Chen, K. Song, W. Bai, J. Yang, Y. Zhang, P. Xiang, *et al.*, "Effect of Nb and more Fe ions co-doping on the microstructures, magnetic, and piezoelectric properties of Aurivillius Bi5Ti3FeO15 phases," *Journal of Applied Physics*, vol. 120, p. 214104, 2016.

[23] C. Lavado and M. G. Stachiotti, "Fe3+/Nb5+ co-doping effects on the properties of Aurivillius Bi4Ti3O12 ceramics," *Journal of Alloys and Compounds*, vol. 731, pp. 914-919, 2018/01/15/ 2018.

[24] X. Liu, L. Xu, Y. Huang, C. Qin, L. Qin, and H. J. Seo, "Improved photochemical properties of Aurivillius Bi 5 Ti 3 FeO 15 with partial substitution of Ti 4+ with Fe 3+," *Ceramics International*, vol. 43, pp. 12372-12380, 2017.

[25] L. Keeney, S. Kulkarni, N. Deepak, M. Schmidt, N. Petkov, P. F. Zhang, *et al.*, "Room temperature ferroelectric and magnetic investigations and detailed phase analysis of Aurivillius phase Bi5Ti3Fe0.7Co0.3O15 thin films," *Journal of Applied Physics*, vol. 112, p. 052010, 2012.

[26] L. Keeney, C. Groh, S. Kulkarni, S. Roy, M. E. Pemble, and R. W. Whatmore, "Room temperature electromechanical and magnetic investigations of ferroelectric Aurivillius phase Bi5Ti3(FexMn1−x)O15 (x = 1 and 0.7) chemical solution deposited thin films," *Journal of Applied Physics*, vol. 112, p. 024101, 2012/07/15 2012.

[27] B. J. Rodriguez, C. Callahan, S. V. Kalinin, and R. Proksch, "Dual-frequency resonance-tracking atomic force microscopy," *Nanotechnology*, vol. 18, p. 475504, 2007.

[28] T. Maity, S. Goswami, D. Bhattacharya, and S. Roy, "Superspin glass mediated giant spontaneous exchange bias in a nanocomposite of BiFeO 3− Bi 2 Fe 4 O 9," *Physical review letters*, vol. 110, p. 107201, 2013.

[29] F. K. Lotgering, "Topotactical reactions with ferrimagnetic oxides having hexagonal crystal structures—I," *Journal of Inorganic and Nuclear Chemistry*, vol. 9, pp. 113-123, 1959/02/01/ 1959.

[30] K. Momma and F. Izumi, "VESTA 3 for three-dimensional visualization of crystal, volumetric and morphology data," *Journal of applied crystallography*, vol. 44, pp. 1272-1276, 2011.

[31] C. H. Hervoches, A. Snedden, R. Riggs, S. H. Kilcoyne, P. Manuel, and P. Lightfoot, "Structural Behavior of the Four-Layer Aurivillius-Phase Ferroelectrics SrBi4Ti4O15 and Bi5Ti3FeO15," *Journal of Solid State Chemistry*, vol. 164, pp. 280-291, 2002.

[32] D. Y. Suárez, I. M. Reaney, and W. E. Lee, "Relation between tolerance factor and Tc in Aurivillius compounds," *Journal of Materials Research*, vol. 16, pp. 3139-3149, 2011.

[33] J. B. Goodenough, "Electronic and ionic transport properties and other physical aspects of perovskites," *Reports on Progress in Physics*, vol. 67, pp. 1915-1993, 2004.

[34] P. Scherrer, "Nachr Ges wiss goettingen," *Math. Phys.*, vol. 2, pp. 98-100, 1918.

[35] R. A. Armstrong and R. E. Newnham, "Bismuth titanate solid solutions," *Materials Research Bulletin*, vol. 7, pp. 1025-1034, 1972/10/01/ 1972.

[36] G. Naresh and T. K. Mandal, "Excellent Sun-Light-Driven Photocatalytic Activity by Aurivillius Layered Perovskites, Bi5–xLaxTi3FeO15 (x = 1, 2)," *ACS Applied Materials & Interfaces*, vol. 6, pp. 21000-21010, 2014/12/10 2014.

[37] J. S. Jang, S. S. Yoon, P. H. Borse, K. T. Lim, T. E. Hong, E. D. Jeong, *et al.*, "Synthesis and characterization of aurivillius phase Bi5Ti3FeO15 layered perovskite for visible light photocatalysis," *Journal of the Ceramic Society of Japan*, vol. 117, pp. 1268-1272, 2009.

[38] Y. Hu, L. Mao, X. Guan, K. A. Tucker, H. Xie, X. Wu, *et al.*, "Layered perovskite oxides and their derivative nanosheets adopting different modification strategies towards better photocatalytic performance of water splitting," *Renewable and Sustainable Energy Reviews*, vol. 119, p. 109527, 2020/03/01/ 2020.

[39] L. Jiang, S. Ni, G. Liu, and X. Xu, "Photocatalytic hydrogen production over Aurivillius compound Bi3TiNbO9 and its modifications by Cr/Nb co-doping," *Applied Catalysis B: Environmental*, vol. 217, pp. 342-352, 2017.

[40] L. Cao, Z. Ding, X. Liu, J. Ren, Y. Chen, M. Ouyang, *et al.*, "Photovoltaic properties of Aurivillius Bi4NdTi3FeO15 ceramics with different orientations," *Journal of Alloys and Compounds*, vol. 800, pp. 134-139, 2019.

[41] S. Sun, W. Wang, H. Xu, L. Zhou, M. Shang, and L. Zhang, "Bi5FeTi3O15 Hierarchical Microflowers: Hydrothermal Synthesis, Growth Mechanism, and Associated Visible-Light-Driven Photocatalysis," *The Journal of Physical Chemistry C*, vol. 112, pp. 17835-17843, 2008/11/20 2008.

[42] D. L. Wood and J. Tauc, "Weak Absorption Tails in Amorphous Semiconductors," *Physical Review B*, vol. 5, pp. 3144-3151, 04/15/ 1972.

[43] M. Wu, Z. Tian, S. Yuan, and Z. Huang, "Magnetic and optical properties of the Aurivillius phase Bi5Ti3FeO15," *Materials Letters*, vol. 68, pp. 190-192, 2012/02/01/ 2012.

[44] W. Bai, Y. Q. Gao, J. Y. Zhu, X. J. Meng, T. Lin, J. Yang, *et al.*, "Electrical, magnetic, and optical properties in multiferroic Bi5Ti3FeO15 thin films prepared by a chemical solution deposition route," *Journal of Applied Physics*, vol. 109, p. 064901, 2011.

[45] R. E. Newnham, R. W. Wolfe, and J. F. Dorrian, "Structural basis of ferroelectricity in the bismuth titanate family," *Materials Research Bulletin*, vol. 6, pp. 1029-1039, 1971/10/01/ 1971.

[46] L. Keeney, R. J. Smith, M. Palizdar, M. Schmidt, A. J. Bell, J. N. Coleman, *et al.*, "Ferroelectric Behavior in Exfoliated 2D Aurivillius Oxide Flakes of Sub-Unit Cell Thickness," *Advanced Electronic Materials*, vol. n/a, p. 1901264, 2020/01/30 2020.

[47] Y. Chen, J. Xu, S. Xie, Z. Tan, R. Nie, Z. Guan, *et al.*, "Ion Doping Effects on the Lattice Distortion and Interlayer Mismatch of Aurivillius-Type Bismuth Titanate Compounds," *Materials (Basel, Switzerland)*, vol. 11, p. 821, 2018.

[48] J. Yuan, R. Nie, Q. Chen, J. Xing, and J. Zhu, "Evolution of structural distortion and electric properties of BTN-based high-temperature piezoelectric ceramics with tungsten substitution," *Journal of Alloys and Compounds*, vol. 785, pp. 475-483, 2019.

[49] Y. Bai, J. Chen, R. Tian, and S. Zhao, "Enhanced multiferroic and magnetoelectric properties of Ho, Mn co-doped Bi5Ti3FeO15 films," *Materials Letters*, vol. 164, pp. 618-622, 2016/02/01/ 2016.

[50] Z. Peng, D. Yan, Q. Chen, D. Xin, D. Liu, D. Xiao, *et al.*, "Crystal structure, dielectric and piezoelectric properties of Ta/W codoped Bi3TiNbO9 Aurivillius phase ceramics," *Current Applied Physics*, vol. 14, pp. 1861-1866, 2014/12/01/ 2014.

[51] X. Mao, W. Wang, H. Sun, Y. Lu, and X. Chen, "Influence of different synthesizing steps on the multiferroic properties of Bi5Fe1Ti3O15 and Bi5Fe0.5Co0.5Ti3O15 ceramics," *Journal of Materials Science*, vol. 47, pp. 2960-2965, 2012/03/01 2012.

[52] D. P. Song, J. Yang, Y. X. Wang, J. Yang, and X. B. Zhu, "Magnetic and ferroelectric properties of Aurivillius phase Bi7Fe3Ti3O21 and their doped films," *Ceramics International*, vol. 43, pp. 17148-17152, 2017.

[53] X. Chen, X. B. Zeng, F. Yang, X. Kong, C. Wei, and P. Su, "Room temperature magnetoelectric coupling in Bi5Ti3FeO15 ceramics," in *Advanced Materials Research*, 2013, pp. 762-766.

[54] H. Sun, X. Lu, J. Su, T. Xu, C. Ju, F. Huang, *et al.*, "Multiferroic behaviour and the magneto-dielectric effect in Bi5FeTi3O15thin films," *Journal of Physics D: Applied Physics*, vol. 45, p. 385001, 2012/09/03 2012.

[55] N. A. Lomanova, V. G. Semenov, V. V. Panchuk, and V. V. Gusarov, "Structural changes in the homologous series of the Aurivillius phases Bin+1Fen−3Ti3O3n+3," *Journal of Alloys and Compounds*, vol. 528, pp. 103-108, 2012/07/05/ 2012.

[56] G. Catalan and J. F. Scott, "Physics and Applications of Bismuth Ferrite," *Advanced Materials*, vol. 21, pp. 2463-2485, 2009/06/26 2009.

[57] T. Kikuchi, "Stability of layered bismuth compounds in relation to the structural mismatch," *Materials Research Bulletin*, vol. 14, pp. 1561-1569, 1979/12/01/ 1979.

[58] A. T. Giddings, M. C. Stennett, D. P. Reid, E. E. McCabe, C. Greaves, and N. C. Hyatt, "Synthesis, structure and characterisation of the n=4 Aurivillius phase Bi5Ti3CrO15," *Journal of Solid State Chemistry*, vol. 184, pp. 252-263, 2011/02/01/ 2011.

[59] I. Vrejoiu, M. Ziese, A. Setzer, P. D. Esquinazi, B. I. Birajdar, A. Lotnyk, *et al.*, "Interfacial strain effects in epitaxial multiferroic heterostructures of Pb Zr x Ti 1− x O 3⁄ La 0.7 Sr 0.3 Mn O 3 grown by pulsed-laser deposition," *Applied Physics Letters*, vol. 92, p. 152506, 2008.

[60] J. Xiong, T. Lei, J. Chu, C. Yang, J. Wei, M. Zhuo, *et al.*, "Ferromagnetic–Antiferromagnetic Coupling by Distortion of Fe/Mn Oxygen Octahedrons in (BiFeO3) m (La0. 7Sr0. 3MnO3) n Superlattices," *Small*, vol. 13, p. 1700107, 2017.